Report

Current Biology

RPL10L Is Required for Male Meiotic Division by Compensating for RPL10 during Meiotic Sex Chromosome Inactivation in Mice

Highlights

- *Rpl10l* is essential for the transition from prophase to metaphase in male meiosis I
- *Rpl10l* expression compensates for *Rpl10* silencing resulting from MSCI
- Ectopically expressed RPL10L can substitute for RPL10 in cultured somatic cells
- *Rpl10* transgenic expression restores spermatogenesis and fertility of *Rpl10l*$^{-/-}$ males

Authors

Long Jiang, Tao Li, Xingxia Zhang, ..., P. Jeremy Wang, Yuanwei Zhang, Qinghua Shi

Correspondence

zyuanwei@ustc.edu.cn (Y.Z.), qshi@ustc.edu.cn (Q.S.)

In Brief

Jiang et al. show that RPL10L is required for the transition from prophase to metaphase in male meiosis I by compensating for RPL10 inactivation resulting from MSCI. The authors provide direct evidence for an X-to-autosome retrogene compensatory hypothesis and novel insight into the functions of these retrogenes in spermatogenesis.

Jiang et al., 2017, Current Biology *27*, 1498–1505
May 22, 2017
http://dx.doi.org/10.1016/j.cub.2017.04.017

CellPress

CellPress

Current Biology
Report

RPL10L Is Required for Male Meiotic Division by Compensating for RPL10 during Meiotic Sex Chromosome Inactivation in Mice

Long Jiang,[1,7] Tao Li,[1,7] Xingxia Zhang,[1] Beibei Zhang,[1] Changping Yu,[1] Yang Li,[1] Suixing Fan,[1] Xiaohua Jiang,[1] Teka Khan,[1] Qiaomei Hao,[1] Peng Xu,[1] Daita Nadano,[2] Mahmoud Huleihel,[3] Eitan Lunenfeld,[4] P. Jeremy Wang,[5] Yuanwei Zhang,[1,*] and Qinghua Shi[1,6,8,*]

[1]USTC-SJH Joint Center for Human Reproduction and Genetics, The CAS Key Laboratory of Innate Immunity and Chronic Diseases, Hefei National Laboratory for Physical Sciences at Microscale, CAS Center for Excellence in Molecular Cell Science, School of Life Sciences, University of Science and Technology of China, Hefei, 230027 Anhui, China
[2]Department of Applied Molecular Biosciences, Graduate School of Bioagricultural Sciences, Nagoya University, Nagoya 464-8601, Japan
[3]The Shraga Segal Department of Microbiology, Immunology and Genetics, The Center of Advanced Research and Education in Reproduction (CARER), Faculty of Health Sciences, Ben-Gurion University of the Negev, Beer-Sheva 84990, Israel
[4]The Center of Advanced Research and Education in Reproduction (CARER), Faculty of Health Sciences, Fertility and IVF Unit, Department of OB/GYN, Soroka Medical Center and Faculty of Health Sciences, Ben-Gurion University of Negev, Beer-Sheva 84990, Israel
[5]Department of Biomedical Sciences, University of Pennsylvania School of Veterinary Medicine, Philadelphia, PA 19104, USA
[6]Collaborative Innovation Center of Genetics and Development, School of Life Sciences, Fudan University, Shanghai 200438, China
[7]These authors contributed equally
[8]Lead Contact
*Correspondence: zyuanwei@ustc.edu.cn (Y.Z.), qshi@ustc.edu.cn (Q.S.)
http://dx.doi.org/10.1016/j.cub.2017.04.017

SUMMARY

The mammalian sex chromosomes have undergone profound changes during their evolution from an ancestral pair of autosomes [1–4]. Specifically, the X chromosome has acquired a paradoxical sex-biased function by redistributing gene contents [5, 6] and has generated a disproportionately high number of retrogenes that are located on autosomes and exhibit male-biased expression patterns [6]. Several selection-based models have been proposed to explain this phenomenon, including a model of sexual antagonism driving X inactivation (SAXI) [6–8] and a compensatory mechanism based on meiotic sex chromosome inactivation (MSCI) [6, 8–11]. However, experimental evidence correlating the function of X-chromosome-derived autosomal retrogenes with evolutionary forces remains limited [12–17]. Here, we show that the deficiency of *Rpl10l*, a murine autosomal retrogene of *Rpl10* with testis-specific expression, disturbs ribosome biogenesis in late-prophase spermatocytes and prohibits the transition from prophase into metaphase of the first meiotic division, resulting in male infertility. *Rpl10l* expression compensates for the lack of *Rpl10*, which exhibits a broad expression pattern but is subject to MSCI during spermatogenesis. Importantly, ectopic expression of *RPL10L* prevents the death of cultured *RPL10*-deficient somatic cells, and *Rpl10l*-promoter-driven transgenic expression of *Rpl10* in spermatocytes restores spermatogenesis and fertility in *Rpl10l*-deficient mice. Our results demonstrate that *Rpl10l* plays an essential role during the meiotic stage of spermatogenesis by compensating for MSCI-mediated transcriptional silencing of *Rpl10*. These data provide direct evidence for the compensatory hypothesis and add novel insight into the evolution of X-chromosome-derived autosomal retrogenes and their role in male fertility.

RESULTS AND DISCUSSION

Rpl10l-Deficient Mice Exhibit Spermatogenic Failure and Male Infertility

The X chromosome evolved dramatically after the divergence of eutherian and metatherian mammals, with two major bursts of gene origination events that resulted in a substantial increase in its contribution to the genome [5]. Concomitantly, a disproportionally high number of retrogenes moved from the X chromosome to the autosomes in the eutherian and metatherian lineages [6, 10]. The observation that these autosomal retrogenes exhibit largely male-biased expression patterns suggests that evolutionary selection forces contributed to this nonrandom gene traffic [5–11]. To date, the function of only a small number of X-to-autosome retrogenes has been investigated [12–17], and insight into the forces that drive directional gene movement during mammalian evolution remains limited.

RPL10L is a testis-specific retrogene originating from *RPL10*, an ancient X-linked ribosomal protein-encoding gene, shortly after the divergence of eutherian and metatherian lineages [5, 18]. In order to further understand the functional association between X-derived retrogenes and its parental paralogs, we selected the *RPL10L* and *RPL10* as a model to investigate their gene expression patterns and functional roles, respectively. Consistent with previous reports [5, 18], we confirmed that *RPL10L* expression

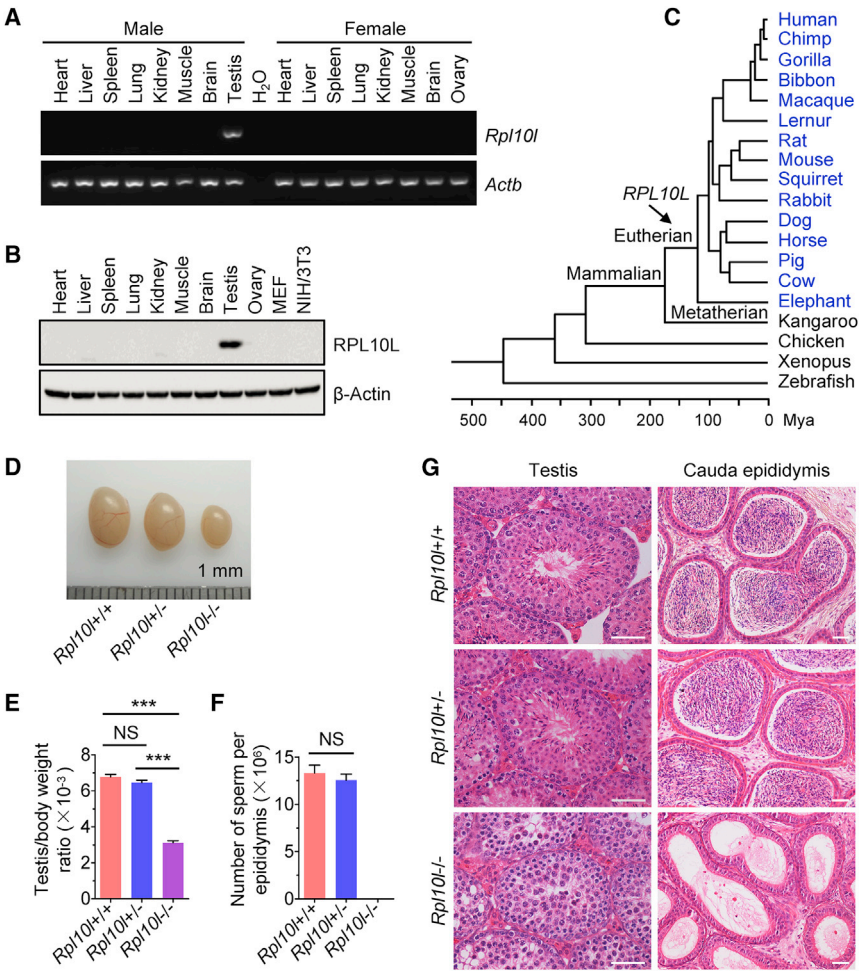

Figure 1. Eutherian-Specific *Rpl10l* Is Expressed Specifically in Mouse Testis and Is Required for Spermatogenesis and Male Fertility

(A) RT-PCR analysis of *Rpl10l* expression in different tissues from adult mice.

(B) Western blot analysis of RPL10L expression in adult mouse tissues and murine cell lines.

(C) Evolution of the *RPL10L* retrogene in vertebrates (blue, present). Phylogenetic tree of vertebrate species with divergence time based on [5, 19, 20]. See also Table S1.

(D–F) Testis morphology (D), ratios of testis weight to body weight (E), and sperm counts (F) of 12-week-old $Rpl10l^{+/+}$, $Rpl10l^{+/-}$, and $Rpl10l^{-/-}$ mice. For (D), see also Figure S1F.

(G) H&E staining of testicular and epididymal sections from 12-week-old $Rpl10l^{+/+}$, $Rpl10l^{+/-}$, and $Rpl10l^{-/-}$ mice. Scale bars represent 50 μm. See also Figure S1G.

Data are representative of two independent experiments in (A) and (B) and at least three independent experiments in (D) and (G). Data are presented as mean ± SEM of at least four mice in (E) and (F). ***$p < 0.001$; NS, $p > 0.05$.

is restricted to the testis in mouse and human (Figures 1A and 1B; Figure S1A) and that orthologs of *RPL10L* exist only in eutherians (Figure 1C; Table S1).

To understand the function of *Rpl10l* during spermatogenesis, we generated *Rpl10l*-deficient mice using CRISPR/Cas9 technology and obtained two mutant strains deleting 70 bp and 59 bp from the sequence of *Rpl10l* gene, respectively (Figures S1B–S1D). Loss of RPL10L protein was confirmed by western blotting of testes from $Rpl10l^{-/-}$ strains 1 and 2 mice (Figure S1E). $Rpl10l^{+/-}$ and $Rpl10l^{-/-}$ mice of both strains were viable and indistinguishable in behavior from $Rpl10l^{+/+}$ mice.

However, $Rpl10l^{-/-}$ males of both strains exhibited similar characteristics of testicular hypoplasia (Figures S1F and S1G). For subsequent studies, we focused on strain 1 containing a 70-bp deletion (hereinafter referred to as $Rpl10l^{-/-}$). The testes from adult $Rpl10l^{-/-}$ mice were substantially smaller than those from their $Rpl10l^{+/-}$ littermates and $Rpl10l^{+/+}$ mice (Figures 1D and 1E). In addition, comparable sperm counts were observed in the cauda epididymides from $Rpl10l^{+/+}$ and $Rpl10l^{+/-}$ mice, whereas the epididymides of $Rpl10l^{-/-}$ animals were devoid of sperm (Figures 1F and 1G). Mating tests confirmed that $Rpl10l^{-/-}$ males were infertile (zero litters in three mating tests with three females per male). These findings indicate that *Rpl10l* is essential for spermatogenesis.

Rpl10l-Deficient Spermatocytes Fail in the Transition from Prophase to Metaphase of Meiosis I

To determine the stage of spermatogenic arrest in $Rpl10l^{-/-}$ mice, we examined testis tissue morphology using H&E-stained sections. Various stages of spermatogenic cells were observed in the seminiferous tubules of $Rpl10l^{+/+}$ and $Rpl10l^{+/-}$ testis tissue, whereas no spermatids and sperm were detectable in $Rpl10l^{-/-}$ testis (Figure 1G), indicating that spermatogenesis did not proceed beyond meiosis in the absence of *Rpl10l*. Immunostaining for PNA, an acrosomal marker identifying spermatid and sperm [21], confirmed the absence of postmeiotic germ cells in $Rpl10l^{-/-}$ testis (Figure 2A).

To determine which step of meiosis was disrupted in $Rpl10l^{-/-}$ mice, we investigated the progression of meiotic prophase I using the spermatocyte micro-spreading method [22]. The percentage of $Rpl10l^{-/-}$ spermatocytes in each successive stage (leptotene, zygotene, pachytene, and diplotene) was comparable to those of $Rpl10l^{+/-}$ spermatocytes (Figures 2B and 2C), indicating that the progression of prophase I was not affected following the deletion of *Rpl10l*. We next examined the progression from prophase to metaphase of meiosis I using the meiotic delay assay [23]. Testes from adult $Rpl10l^{-/-}$ males contained significantly fewer spermatocytes in the first meiotic metaphase (MMI) than testes from $Rpl10l^{+/-}$ littermates (Figure 2D), indicating that spermatogenesis was arrested at the transition from prophase I to metaphase I. This finding was confirmed by histological analysis of the first wave of spermatogenesis. Periodic acid-Schiff (PAS) staining of testicular sections revealed no obvious differences between $Rpl10l^{-/-}$ and $Rpl10l^{+/-}$ testes at 15 days post-partum (dpp) (Figure S2A). In seminiferous

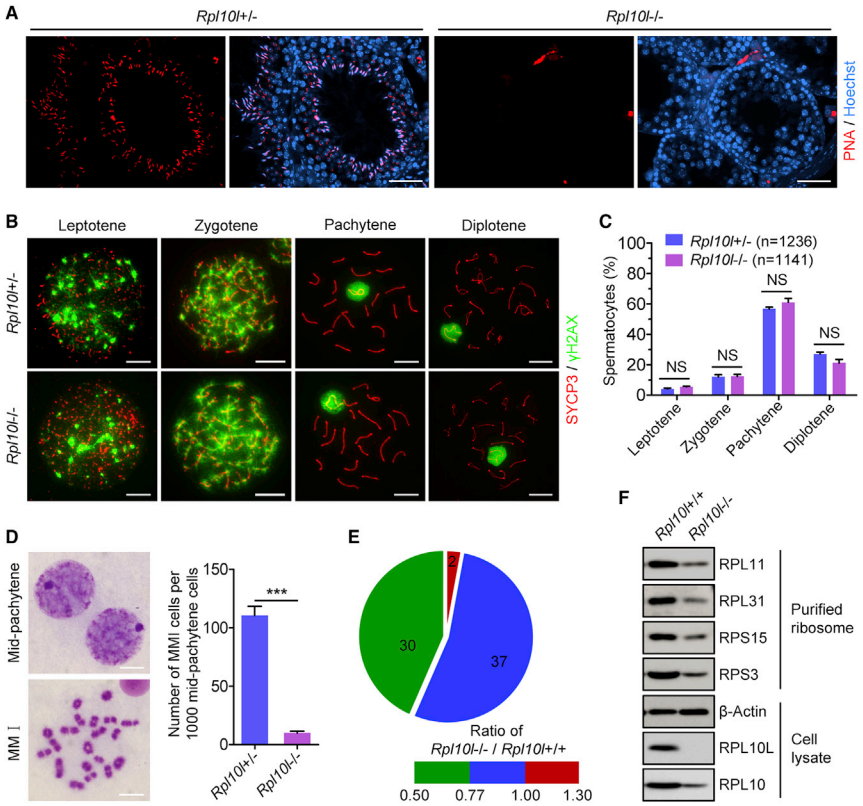

Figure 2. *Rpl10l* Deletion Causes Failure of the First Meiotic Division and Disrupts Ribosome Biogenesis

(A) PNA immunostaining (red) of testicular sections from adult *Rpl10l*$^{+/-}$ and *Rpl10l*$^{-/-}$ mice. Nuclei were counterstained with Hoechst 33342 (blue).

(B) Immunostaining of surface-spread spermatocytes from adult *Rpl10l*$^{+/-}$ and *Rpl10l*$^{-/-}$ mice for SYCP3 (red) and γH2AX (green).

(C) Percentages of spermatocytes at successive stages of meiotic prophase I as shown in (B).

(D) Number of MMI cells relative to 1,000 mid-pachytene spermatocytes per animal of the indicated genotypes.

(E) Expression changes in ribosomal proteins in late-prophase *Rpl10l*$^{-/-}$ versus *Rpl10l*$^{+/+}$ spermatocytes as determined by quantitative proteomic analysis. See also Figure S2I and Table S3.

(F) Western blot analysis demonstrating lower yield of ribosomes from late-prophase *Rpl10l*$^{-/-}$ compared with *Rpl10l*$^{+/+}$ spermatocytes. The RPL10 antibody (Novus Biologicals, NBP1-84037) recognizes both RPL10 and RPL10L.

Data are representative of at least two independent experiments in (A), (B), and (F). Data are presented as mean ± SEM of four mice with a similar number of cells scored per animal in (C) (n, total number of cells that were scored) and presented as mean ± SEM of three mice in (D). ***$p < 0.001$; NS, $p > 0.05$. Scale bars represent 50 μm in (A) and 10 μm in (B) and (D).

tubules of *Rpl10l*$^{+/-}$ testes, MMI spermatocytes were observed at 21 dpp and 27 dpp, and elongated spermatids were seen at 27 dpp, whereas these cells were not present in *Rpl10l*$^{-/-}$ testes (Figure S2A). Instead, seminiferous tubules of *Rpl10l*$^{-/-}$ testes contained spermatocytes with highly condensed chromatin (Figure S2A). Furthermore, TUNEL assay showed a significant increase in the number of apoptotic spermatocytes in *Rpl10l*$^{-/-}$ testes (Figures S2B–S2D). Taken together, these analyses confirm a pivotal role of RPL10L during the first meiotic division of spermatocytes.

It has been reported that several X-chromosome-derived autosomal retrogenes play essential roles in spermatogenesis. *Utp14b* deficiency results in male infertility in adult mice due to mitotic arrest in type A spermatogonia [24, 25]. *Pgk2*, *Cetn1*, and *Cstf2t* are essential for late steps of spermiogenesis or sperm maturation, but their deletion does not affect meiosis [12–14]. Heterozygous deletion of *Hnrnpgt* leads to spermatogenic failure in mice, but the functional role of this gene remains unknown [15]. To our knowledge, *Rpl10l* is the first known X-chromosome-derived autosomal retrogene that is required for meiotic progression during spermatogenesis.

Rpl10l Deletion Disrupts Ribosome Biogenesis in Late-Prophase Spermatocytes

To understand how *Rpl10l* deletion results in spermatogenic failure, we compared global protein expression profiles of late-prophase (pachytene and diplotene) *Rpl10l*$^{-/-}$ and *Rpl10l*$^{+/+}$ spermatocytes isolated by STA-PUT [26, 27]. The proportions of pachytene and diplotene spermatocytes in isolates from *Rpl10l*$^{-/-}$ testes were comparable to those from *Rpl10l*$^{+/+}$ testes (Figures S2E–S2G). Using TMT (tandem mass tag)-based quantitative proteomic analysis, we quantified a total of 3,100 proteins with a minimum of two unique peptides. Of these, 445 proteins were downregulated (*Rpl10l*$^{-/-}$/*Rpl10l*$^{+/+}$ ratio < 0.77) and 368 proteins were upregulated (*Rpl10l*$^{-/-}$/*Rpl10l*$^{+/+}$ ratio > 1.3) in late-prophase *Rpl10l*$^{-/-}$ versus *Rpl10l*$^{+/+}$ spermatocytes (Table S2). Notably, the levels of several proteins known to be necessary for the progression from prophase to metaphase of male mouse meiosis I—including NEK2, HSPA2, CCNA1, PLK1, and CKS2 [28–33]—were decreased (Figure S2H; Table S2). These disturbances in protein levels were likely associated with spermatogenic failure and apoptosis of spermatocytes in *Rpl10l*$^{-/-}$ mice.

Because RPL10L is a ribosomal component in mouse spermatogenic cells [34, 35], we assessed the levels of ribosomal proteins in the quantitative proteomics data. Out of a total of 69 ribosomal proteins identified, 67 exhibited lower levels in *Rpl10l*$^{-/-}$ compared with *Rpl10l*$^{+/+}$ late-prophase spermatocytes, including 30 proteins with a more than 1.3-fold decrease and 37 proteins with a less than 1.3-fold decrease (Figures 2E and S2I; Table S3). Disturbances in ribosome biogenesis were further confirmed by a low ribosome yield from late-prophase spermatocytes of *Rpl10l*$^{-/-}$ mice (Figure 2F). These observations were consistent with previous reports that deletion of a ribosomal protein abrogates ribosome biogenesis and leads to a decrease in the level of other ribosomal proteins [36–38]. These results indicate that RPL10L is essential for ribosome biogenesis and the maintenance of steady-state levels of proteins required for the progression of meiosis.

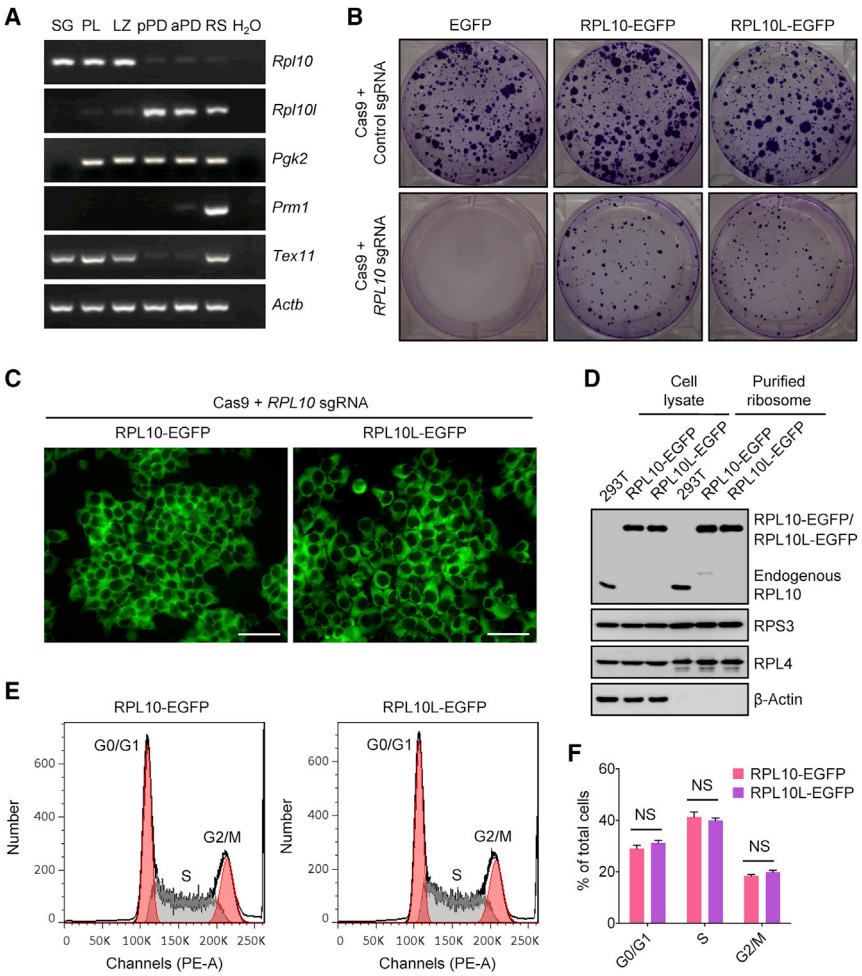

Figure 3. *Rpl10l* Appears to Compensate for *Rpl10* Silencing during Spermatogenesis

(A) RT-PCR analysis of *Rpl10* and *Rpl10l* transcript levels in purified mouse spermatogenic cell populations. SG, spermatogonia (type A); PL, preleptotene spermatocytes; LZ, leptotene plus zygotene spermatocytes; pPD, pubertal pachytene plus diplotene spermatocytes; aPD, adult pachytene plus diplotene spermatocytes; RS, round spermatids. Cell population analysis is as described in Figures S3C and S3D.

(B) Representative images of crystal-violet-stained 293T clones after co-transfection with expression vectors encoding CRISPR/Cas9 system components and EGFP-tagged proteins (as indicated), followed by puromycin and blasticidin selection for 12 days.

(C) EGFP expression in cells surviving after co-transfection of *RPL10*-targeted CRISPR/Cas9 and RPL10-EGFP or RPL10L-EGFP expression vectors as shown in (B). Scale bars, 50 μm.

(D) Western blot analysis of RPL10 and RPL10L in cell lysates and purified ribosomes from surviving cells shown in (C). 293T cells serve as the positive control for endogenous RPL10. The RPL10 antibody (Novus Biologicals, NBP1-84037) recognizes both RPL10 and RPL10L.

(E and F) Flow-cytometric cell-cycle analysis of surviving cells shown in (C). Representative flow-cytometry histograms are presented in (E), and frequencies of cell subpopulations in cell-cycle phases G0/G1, S, and G2/M are presented in (F). Data are representative of two or three independent experiments in (A)–(E) and are presented as mean ± SEM of three independent experiments, with biological duplicates in (F). NS, $p > 0.05$.

Rpl10 Expression Is Subject to Meiotic Sex Chromosome Inactivation

Rpl10, the ancient progenitor gene of *Rpl10l*, is highly conserved from yeast to human and locates on the X chromosome in vertebrates. Given that the X chromosome tends to be feminized by enriching female-biased genes and dislodging the male-biased genes due to its longer stay time in females according to the SAXI hypothesis [5–8, 39, 40], we assessed the expression pattern of *Rpl10* in both sexes. RT-PCR and qPCR results revealed that *Rpl10* is broadly expressed in different tissues with similar expression levels between male and female mice, except for a relatively lower expression in testis (Figures S3A and S3B). Considering that *Rpl10* may be subject to meiotic sex chromosome inactivation (MSCI), which results in the transcriptional silencing of most protein-coding genes on the sex chromosomes from the pachytene stage until spermiogenesis [11, 41–44], we examined the expression dynamics of *Rpl10* in mouse germ cell populations isolated by STA-PUT (Figures S3C and S3D). RT-PCR analysis showed that the expression level of *Rpl10* was comparable in spermatogonia and early spermatocytes (preleptotene to zygotene) but sharply reduced in late spermatocytes (pachytene and diplotene) and round spermatids (Figure 3A), indicating transcriptional silencing of *Rpl10* during and after MSCI. Silencing of *Rpl10* may explain the relatively lower expression level detected in testis.

RPL10 Is Essential for Ribosome Biogenesis and Cell Proliferation

RPL10 is one of the last proteins to assemble into the nascent 60S subunit of ribosome and is essential for protein synthesis and population-replicative lifespan in yeast [45–47]. In human and mouse, assembly of the RPL10 protein into the 60S subunit only occurs in the cytoplasm [34, 35, 48]. To investigate the effect of *RPL10* knockdown on ribosome biogenesis in mammalian cells, we analyzed polysome profiles from extracts of cultured human cells transfected with *RPL10*-targeted small interfering RNAs (siRNAs). Knockdown of *RPL10* resulted in decreased levels of 60S ribosomal subunits, 80S ribosomes, and polysomes (Figure S3E), indicating a disturbance of ribosome biogenesis. As expected, the levels of other ribosomal proteins were decreased in *RPL10*-knockdown cells (Figure S3F), ultimately resulting in G1 cell-cycle arrest (Figure S3G). To further determine the effect of *RPL10* deletion in cell proliferation, we generated a cell line that lacked endogenous *RPL10* and stably expressed tetracycline-inducible (Tet-On) RPL10-EGFP and performed clone formation assays. An abundance of clones survived in cultures treated with doxycycline, while no clones were observed in the

non-doxycycline group (Figures S3H and S3I). These results, together with its expression pattern, indicate that RPL10 plays a housekeeping role in ribosome biogenesis and cell proliferation.

Rpl10l Expression Compensates for *Rpl10* Silencing during Spermatogenesis

The MSCI-based compensatory hypothesis—i.e., the autosomal retrogenes with male-biased function in late spermatogenesis can compensate for the housekeeping function of their X-linked parental genes—is widely accepted as an explanation for the formation of X-chromosome-derived autosomal retrogenes [6, 8–11]. According to this hypothesis, an increase in *Rpl10l* expression should be observed specifically during and after meiosis when *Rpl10* is silenced by MSCI. To test this hypothesis, we assessed mRNA levels of *Rpl10l* in purified male mouse germ cells of different developmental stages by RT-PCR. *Rpl10l* was highly expressed in late spermatocytes (pachytene and diplotene) and round spermatids but weakly expressed in spermatogonia and early spermatocytes (Figure 3A), exhibiting a strikingly mutually complementary expression pattern with *Rpl10* in male germ cells. This observation is consistent with a previous report that RPL10L staining was observed in spermatogenic cells located in the seminiferous lumen but not in monolayer cells attached to the basement membrane of seminiferous tubules [35]. Thus, we propose that *Rpl10l* compensates for *Rpl10* silencing during spermatogenesis.

Ectopically Expressed RPL10L Can Substitute for RPL10 in Cultured Human Cells

To substantiate that RPL10L can compensate for RPL10 function, we performed a rescue experiment in human cultured cells in which endogenous *RPL10* was disrupted using the CRISPR/Cas9 method. To this end, we co-transfected 293T cells with CRISPR/Cas9 and *RPL10*-targeted single-guide RNA (sgRNA) vectors, in combination with either EGFP, RPL10-EGFP, or RPL10L-EGFP expression vectors. After 12 days of puromycin and blasticidin treatment to select for cell clones retaining both Cas9 and sgRNA constructs, cell cultures transfected with RPL10-EGFP contained multiple surviving cell clones, indicating that ectopic RPL10 compensated for the endogenous gene product as expected (Figure 3B). Interestingly, a similar number of clones survived in cultures transfected with RPL10L-EGFP (Figure 3B). To confirm that the surviving cells were rescued by RPL10L-EGFP expression, we evaluated these clones for GFP fluorescence by microscopy and assessed the expression of endogenous RPL10 and ectopic expression of RPL10L-EGFP by western blotting. All surviving cells expressed RPL10L-EGFP in the cytoplasm and lacked endogenous RPL10 (Figures 3C and 3D), indicating that ectopically expressed RPL10L prevented the death of *RPL10*-deficient cells. More importantly, cell-cycle duration did not differ between cells deficient for endogenous RPL10 that were rescued by either RPL10L-EGFP or RPL10-EGFP expression (Figures 3E and 3F). These results were further confirmed by observations in cells that lacked the endogenous RPL10 and stably expressed Tet-On RPL10L-EGFP. Upon exposure to doxycycline, these cells grew similarly to control cells expressing endogenous RPL10 (Figures S3J and S3K). These results indicate that ectopically expressed RPL10L can substitute for RPL10 in cultured human cells.

Transgenic Expression of *Rpl10-mCherry* Partly Restores Spermatogenesis and Fertility of *Rpl10l*-Deficient Males

To further substantiate that *Rpl10l* plays the same function with *Rpl10* and compensates for *Rpl10* silencing during spermatogenesis, we attempted to use the transgenic *Rpl10* to rescue the spermatogenesis and fertility in *Rpl10l*$^{-/-}$ mice. To achieve this purpose, we first generated a transgenic mouse strain expressing *Rpl10-mCherry* driven by the *Rpl10l* promoter (*Rpl10-mCherry*^{TG}) (Figure S4A). Similar to endogenous RPL10L [35], the RPL10-mCherry protein was detectable only in pachytene spermatocytes and cells at subsequent stages of germ cell development (Figures S4B and S4C).

We then intercrossed *Rpl10-mCherry*^{TG} males with *Rpl10l*$^{-/-}$ females. The F2 generation adult *Rpl10l*$^{-/-}$;*Rpl10-mCherry*^{TG} males exhibited a smaller testis size and lower sperm count than *Rpl10l*$^{+/-}$ and *Rpl10l*$^{+/-}$;*Rpl10-mCherry*^{TG} littermates but had significantly larger testes and higher sperm counts compared with *Rpl10l*$^{-/-}$ littermates (Figures 4A–4C). H&E staining of testicular sections from *Rpl10l*$^{-/-}$;*Rpl10-mCherry*^{TG} mice showed that most seminiferous tubules contained different stages of germ cells (Figure 4D), indicating that spermatogenesis was restored. This was confirmed by a dramatically increased number of MMI spermatocytes in *Rpl10l*$^{-/-}$;*Rpl10-mCherry*^{TG} testis compared to *Rpl10l*$^{-/-}$ testis (Figure 4E). Consistently, the fertility of *Rpl10l*$^{-/-}$;*Rpl10-mCherry*^{TG} males was restored. After mating with *Rpl10l*$^{+/+}$ females, litters from *Rpl10l*$^{-/-}$;*Rpl10-mCherry*^{TG} males had fewer pups than those from *Rpl10l*$^{+/-}$;*Rpl10-mCherry*^{TG} or *Rpl10l*$^{+/-}$ males (Figure 4F); similar results were observed in the next-generation *Rpl10l*$^{-/-}$;*Rpl10-mCherry*^{TG} males (Figure S4D). These findings indicate that transgenic *Rpl10* can partly compensate for *Rpl10l* loss of function.

Noticeably, defects in spermatogenesis were detectable in 27.21% (±7.86% SEM) of seminiferous tubules from *Rpl10l*$^{-/-}$;*Rpl10-mCherry*^{TG} testes (Figure S4E). Coincidently, RPL10-mCherry protein expression was absent in 26.67% (±8.96% SEM) of seminiferous tubules from *Rpl10l*$^{-/-}$;*Rpl10-mCherry*^{TG} testes (Figure S4F), which implies that the observed partial rescue of spermatogenesis in *Rpl10l*$^{-/-}$;*Rpl10-mCherry*^{TG} mice may result from mosaic expression of transgenic *Rpl10-mCherry* in the testis. Based on previous observations [8], we can also not exclude the possibility that *Rpl10l* may have acquired additional functions besides compensation for *Rpl10* since its divergence from *Rpl10*.

Collectively, we have demonstrated that RPL10L plays an essential role during meiosis of spermatogenesis by compensating for its X-linked parental paralog, RPL10, during and after MSCI. First, *Rpl10l* is required for meiotic progression during spermatogenesis. Second, *Rpl10l* exhibited a strikingly mutually complementary expression pattern with *Rpl10* in male germ cells. Third, *RPL10L* can substitute for *RPL10* in cultured human cells, and vice versa—*Rpl10* can complement *Rpl10l* in mice. Based on these results and the known evolution of *RPL10L*, our study substantiates the hypothesis that MSCI plays a critical role for the selective fixation of X-derived autosomal retrogenes in mammals and provides novel insight into these retrogenes' functions in male fertility.

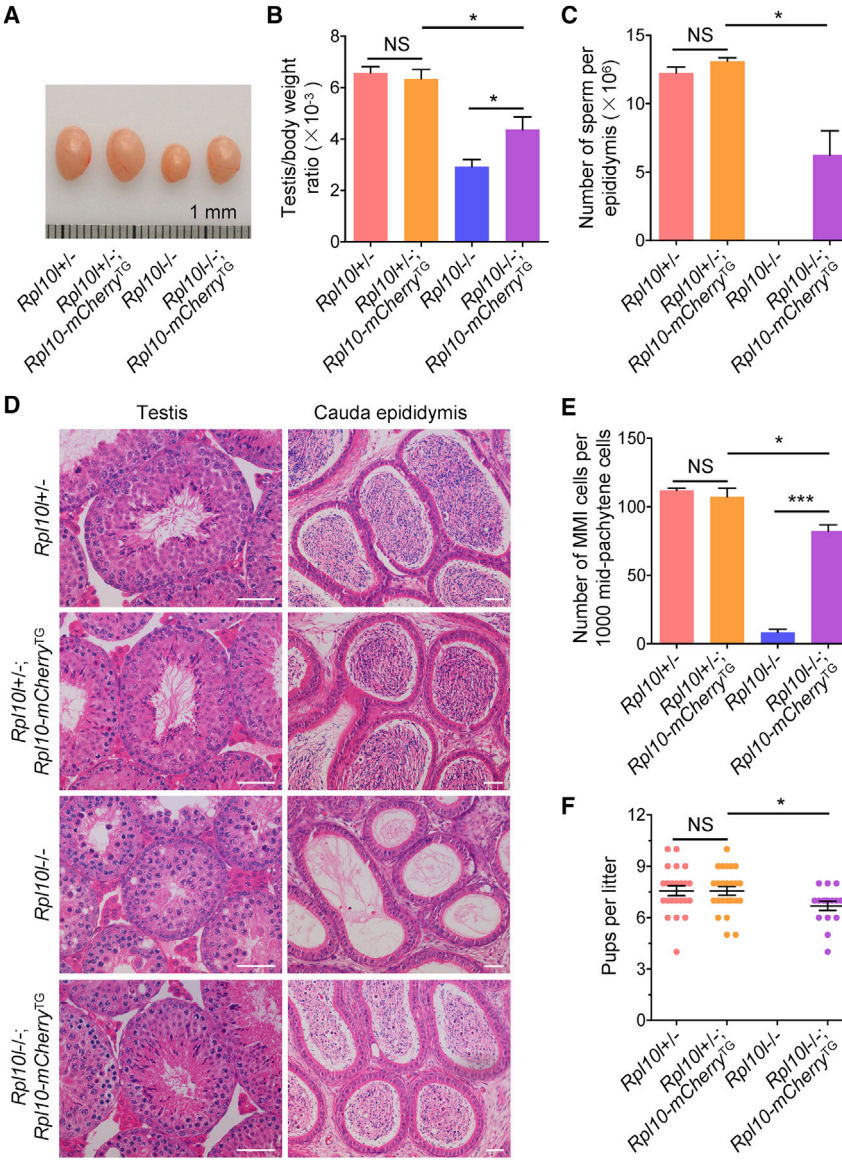

Figure 4. Spermatogenesis and Fertility of *Rpl10l*-Deficient Mice Can Be Restored by Transgenic Expression of *Rpl10*

(A–D) Testis morphology (A), ratios of testis weight to body weight (B), sperm counts (C), and H&E-stained testicular and epididymal sections (D) from 12-week-old *Rpl10l*$^{+/-}$, *Rpl10l*$^{+/-}$;*Rpl10-mCherry*^{TG}, *Rpl10l*$^{-/-}$, and *Rpl10l*$^{-/-}$;*Rpl10-mCherry*^{TG} mice. Scale bars in (D) represent 50 μm.

(E) Number of MMI cells relative to 1,000 mid-pachytene cells per animal of the indicated genotypes.

(F) Litter sizes in mating tests of male mice of the indicated genotype. Each male was mated with three wild-type females. Each dot represents one litter. See also Figure S4D.

Data are representative of three independent experiments in (A) and (D), presented as mean ± SEM of three or four mice in (B), (C), and (E), and presented as mean ± SEM of scored litters from three males per genotype in (F). *$p < 0.05$; ***$p < 0.001$; NS, $p > 0.05$.

STAR★METHODS

Detailed methods are provided in the online version of this paper and include the following:

- KEY RESOURCES TABLE
- CONTACT FOR REAGENT AND RESOURCE SHARING
- EXPERIMENTAL MODEL AND SUBJECT DETAILS
  - Mice
  - Cell culture
- METHOD DETAILS
  - Plasmids
  - Transfection and RNAi
  - RNA extraction, RT-PCR and qPCR
  - Ribosome purification
  - Protein samples and western blot analysis
  - Polysome profiling analysis
  - Flow cytometry
  - Separation of mouse spermatogenic cells
  - Fertility test
  - Histology
  - Sperm counting
  - Meiotic delay assay
  - Spermatocyte micro-spreading and immunostaining
  - TUNEL assay
  - Immunostaining of testis sections
- QUANTIFICATION AND STATISTICAL ANALYSES
  - Quantitative proteomic analysis
  - Statistical analysis
- DATA AND SOFTWARE AVAILABILITY

SUPPLEMENTAL INFORMATION

Supplemental Information includes four figures and four tables and can be found with this article online at http://dx.doi.org/10.1016/j.cub.2017.04.017.

AUTHOR CONTRIBUTIONS

L.J., T.L., and Q.S. designed the research. L.J. and T.L. carried out and analyzed all experiments, with assistance from X.Z. and B.Z. for immunostaining and fertility testing; C.Y., Y.L., and S.F. for plasmid construction and gene-targeted mice; and X.J. and Y.Z. for analysis of proteomics data. D.N. provided the mouse RPL10L antibody. L.J. and Q.S. wrote the manuscript. T.K., Q.H., P.X., D.N., M.H., E.L., P.J.W., and Y.Z. provided critical suggestions for experiment design. All authors read and edited the manuscript. Q.S. supervised the project.

ACKNOWLEDGMENTS

We thank Dr. Howard J. Cooke for valuable suggestions, Dr. Xingxu Huang for plasmids of the CRISPR/Cas9 system and suggestions, Dr. Xiaoyuan Song for the pTRIPZ vector, and Drs. Congzhao Zhou and Rongbin Zhou for allowing us to use Density Gradient Fractionation Systems and the FACSCalibur flow cytometer, respectively. We also thank Xiaoyu Zhang and Hongtao Cheng for the generation and care of genetically modified mice, and Dr. Fang Wang, Dr. Saeed Ahmad, Hanwei Jiang, and other members of the Q.S. lab for comments and advice. This work was supported by the National Key Research and Developmental Program of China (2016YFC1000600); the Strategic Priority Research Program of the Chinese Academy of Sciences (XDB19000000); the Joint NSFC-ISF Research Program, jointly funded by the National Natural Science Foundation of China and the Israel Science Foundation (31461143013); the National Basic Research Program of China (2014CB943101); the National Natural Science Foundation of China (31371519, 31501199, 31301227, and 31571555); the Major Program of Development Foundation of Hefei Centre for Physical Science and Technology (2014FXZY003); and the Fundamental Research Funds for the Central Universities (WK2070000053 and WK2340000069).

Received: December 7, 2016
Revised: March 5, 2017
Accepted: April 11, 2017
Published: May 11, 2017

REFERENCES

1. Schaffner, S.F. (2004). The X chromosome in population genetics. Nat. Rev. Genet. *5*, 43–51.
2. Marshall Graves, J.A. (2002). Sex chromosomes and sex determination in weird mammals. Cytogenet. Genome Res. *96*, 161–168.
3. Skaletsky, H., Kuroda-Kawaguchi, T., Minx, P.J., Cordum, H.S., Hillier, L., Brown, L.G., Repping, S., Pyntikova, T., Ali, J., Bieri, T., et al. (2003). The male-specific region of the human Y chromosome is a mosaic of discrete sequence classes. Nature *423*, 825–837.
4. Lahn, B.T., Pearson, N.M., and Jegalian, K. (2001). The human Y chromosome, in the light of evolution. Nat. Rev. Genet. *2*, 207–216.
5. Zhang, Y.E., Vibranovski, M.D., Landback, P., Marais, G.A., and Long, M. (2010). Chromosomal redistribution of male-biased genes in mammalian evolution with two bursts of gene gain on the X chromosome. PLoS Biol. *8*, e1000494.
6. Emerson, J.J., Kaessmann, H., Betrán, E., and Long, M. (2004). Extensive gene traffic on the mammalian X chromosome. Science *303*, 537–540.
7. Wu, C.I., and Xu, E.Y. (2003). Sexual antagonism and X inactivation–the SAXI hypothesis. Trends Genet. *19*, 243–247.
8. Shiao, M.S., Khil, P., Camerini-Otero, R.D., Shiroishi, T., Moriwaki, K., Yu, H.T., and Long, M. (2007). Origins of new male germ-line functions from X-derived autosomal retrogenes in the mouse. Mol. Biol. Evol. *24*, 2242–2253.
9. Wang, P.J. (2004). X chromosomes, retrogenes and their role in male reproduction. Trends Endocrinol. Metab. *15*, 79–83.
10. Potrzebowski, L., Vinckenbosch, N., Marques, A.C., Chalmel, F., Jégou, B., and Kaessmann, H. (2008). Chromosomal gene movements reflect the recent origin and biology of therian sex chromosomes. PLoS Biol. *6*, e80.
11. Turner, J.M. (2015). Meiotic silencing in mammals. Annu. Rev. Genet. *49*, 395–412.
12. Danshina, P.V., Geyer, C.B., Dai, Q., Goulding, E.H., Willis, W.D., Kitto, G.B., McCarrey, J.R., Eddy, E.M., and O'Brien, D.A. (2010). Phosphoglycerate kinase 2 (PGK2) is essential for sperm function and male fertility in mice. Biol. Reprod. *82*, 136–145.
13. Avasthi, P., Scheel, J.F., Ying, G., Frederick, J.M., Baehr, W., and Wolfrum, U. (2013). Germline deletion of Cetn1 causes infertility in male mice. J. Cell Sci. *126*, 3204–3213.
14. Tardif, S., Akrofi, A.S., Dass, B., Hardy, D.M., and MacDonald, C.C. (2010). Infertility with impaired zona pellucida adhesion of spermatozoa from mice lacking TauCstF-64. Biol. Reprod. *83*, 464–472.
15. Ehrmann, I., Dalgliesh, C., Tsaousi, A., Paronetto, M.P., Heinrich, B., Kist, R., Cairns, P., Li, W., Mueller, C., Jackson, M., et al. (2008). Haploinsufficiency of the germ cell-specific nuclear RNA binding protein hnRNP G-T prevents functional spermatogenesis in the mouse. Hum. Mol. Genet. *17*, 2803–2818.
16. Banks, K.G., Johnson, K.A., Lerner, C.P., Mahaffey, C.L., Bronson, R.T., and Simpson, E.M. (2003). Retroposon compensatory mechanism hypothesis not supported: Zfa knockout mice are fertile. Genomics *82*, 254–260.
17. Bradley, J., Baltus, A., Skaletsky, H., Royce-Tolland, M., Dewar, K., and Page, D.C. (2004). An X-to-autosome retrogene is required for spermatogenesis in mice. Nat. Genet. *36*, 872–876.
18. Uechi, T., Maeda, N., Tanaka, T., and Kenmochi, N. (2002). Functional second genes generated by retrotransposition of the X-linked ribosomal protein genes. Nucleic Acids Res. *30*, 5369–5375.
19. Springer, M.S., and Murphy, W.J. (2007). Mammalian evolution and biomedicine: new views from phylogeny. Biol. Rev. Camb. Philos. Soc. *82*, 375–392.
20. Kumar, S., and Hedges, S.B. (1998). A molecular timescale for vertebrate evolution. Nature *392*, 917–920.
21. Kanemori, Y., Koga, Y., Sudo, M., Kang, W., Kashiwabara, S., Ikawa, M., Hasuwa, H., Nagashima, K., Ishikawa, Y., Ogonuki, N., et al. (2016). Biogenesis of sperm acrosome is regulated by pre-mRNA alternative splicing of Acrbp in the mouse. Proc. Natl. Acad. Sci. USA *113*, E3696–E3705.
22. Yang, Q., Zhang, D., Leng, M., Yang, L., Zhong, L., Cooke, H.J., and Shi, Q. (2011). Synapsis and meiotic recombination in male Chinese muntjac (Muntiacus reevesi). PLoS ONE *6*, e19255.
23. Jiang, X., Ma, T., Zhang, Y., Zhang, H., Yin, S., Zheng, W., Wang, L., Wang, Z., Khan, M., Sheikh, S.W., et al. (2015). Specific deletion of Cdh2 in Sertoli cells leads to altered meiotic progression and subfertility of mice. Biol. Reprod. *92*, 79.
24. Beamer, W.G., Cunliffe-Beamer, T.L., Shultz, K.L., Langley, S.H., and Roderick, T.H. (1988). Juvenile spermatogonial depletion (jsd): a genetic defect of germ cell proliferation of male mice. Biol. Reprod. *38*, 899–908.
25. Rohozinski, J., and Bishop, C.E. (2004). The mouse juvenile spermatogonial depletion (jsd) phenotype is due to a mutation in the X-derived retrogene, mUtp14b. Proc. Natl. Acad. Sci. USA *101*, 11695–11700.
26. Bryant, J.M., Meyer-Ficca, M.L., Dang, V.M., Berger, S.L., and Meyer, R.G. (2013). Separation of spermatogenic cell types using STA-PUT velocity sedimentation. J. Vis. Exp. (80), e50648.
27. Wang, P.J., Page, D.C., and McCarrey, J.R. (2005). Differential expression of sex-linked and autosomal germ-cell-specific genes during spermatogenesis in the mouse. Hum. Mol. Genet. *14*, 2911–2918.
28. Di Agostino, S., Rossi, P., Geremia, R., and Sette, C. (2002). The MAPK pathway triggers activation of Nek2 during chromosome condensation in mouse spermatocytes. Development *129*, 1715–1727.
29. Di Agostino, S., Fedele, M., Chieffi, P., Fusco, A., Rossi, P., Geremia, R., and Sette, C. (2004). Phosphorylation of high-mobility group protein A2 by Nek2 kinase during the first meiotic division in mouse spermatocytes. Mol. Biol. Cell *15*, 1224–1232.

30. Zhu, D., Dix, D.J., and Eddy, E.M. (1997). HSP70-2 is required for CDC2 kinase activity in meiosis I of mouse spermatocytes. Development *124*, 3007–3014.
31. Liu, D., Matzuk, M.M., Sung, W.K., Guo, Q., Wang, P., and Wolgemuth, D.J. (1998). Cyclin A1 is required for meiosis in the male mouse. Nat. Genet. *20*, 377–380.
32. Kim, J., Ishiguro, K., Nambu, A., Akiyoshi, B., Yokobayashi, S., Kagami, A., Ishiguro, T., Pendas, A.M., Takeda, N., Sakakibara, Y., et al. (2015). Meikin is a conserved regulator of meiosis-I-specific kinetochore function. Nature *517*, 466–471.
33. Spruck, C.H., de Miguel, M.P., Smith, A.P., Ryan, A., Stein, P., Schultz, R.M., Lincoln, A.J., Donovan, P.J., and Reed, S.I. (2003). Requirement of Cks2 for the first metaphase/anaphase transition of mammalian meiosis. Science *300*, 647–650.
34. Sugihara, Y., Honda, H., Iida, T., Morinaga, T., Hino, S., Okajima, T., Matsuda, T., and Nadano, D. (2010). Proteomic analysis of rodent ribosomes revealed heterogeneity including ribosomal proteins L10-like, L22-like 1, and L39-like. J. Proteome Res. *9*, 1351–1366.
35. Sugihara, Y., Sadohara, E., Yonezawa, K., Kugo, M., Oshima, K., Matsuda, T., and Nadano, D. (2013). Identification and expression of an autosomal paralogue of ribosomal protein S4, X-linked, in mice: potential involvement of testis-specific ribosomal proteins in translation and spermatogenesis. Gene *521*, 91–99.
36. Volarevic, S., Stewart, M.J., Ledermann, B., Zilberman, F., Terracciano, L., Montini, E., Grompe, M., Kozma, S.C., and Thomas, G. (2000). Proliferation, but not growth, blocked by conditional deletion of 40S ribosomal protein S6. Science *288*, 2045–2047.
37. Robledo, S., Idol, R.A., Crimmins, D.L., Ladenson, J.H., Mason, P.J., and Bessler, M. (2008). The role of human ribosomal proteins in the maturation of rRNA and ribosome production. RNA *14*, 1918–1929.
38. Kirn-Safran, C.B., Oristian, D.S., Focht, R.J., Parker, S.G., Vivian, J.L., and Carson, D.D. (2007). Global growth deficiencies in mice lacking the ribosomal protein HIP/RPL29. Dev. Dyn. *236*, 447–460.
39. Carrel, L., and Willard, H.F. (2005). X-inactivation profile reveals extensive variability in X-linked gene expression in females. Nature *434*, 400–404.
40. Khil, P.P., Smirnova, N.A., Romanienko, P.J., and Camerini-Otero, R.D. (2004). The mouse X chromosome is enriched for sex-biased genes not subject to selection by meiotic sex chromosome inactivation. Nat. Genet. *36*, 642–646.
41. Turner, J.M. (2007). Meiotic sex chromosome inactivation. Development *134*, 1823–1831.
42. Cloutier, J.M., and Turner, J.M. (2010). Meiotic sex chromosome inactivation. Curr. Biol. *20*, R962–R963.
43. Yan, W., and McCarrey, J.R. (2009). Sex chromosome inactivation in the male. Epigenetics *4*, 452–456.
44. Sosa, E., Flores, L., Yan, W., and McCarrey, J.R. (2015). Escape of X-linked miRNA genes from meiotic sex chromosome inactivation. Development *142*, 3791–3800.
45. Hedges, J., West, M., and Johnson, A.W. (2005). Release of the export adapter, Nmd3p, from the 60S ribosomal subunit requires Rpl10p and the cytoplasmic GTPase Lsg1p. EMBO J. *24*, 567–579.
46. West, M., Hedges, J.B., Chen, A., and Johnson, A.W. (2005). Defining the order in which Nmd3p and Rpl10p load onto nascent 60S ribosomal subunits. Mol. Cell. Biol. *25*, 3802–3813.
47. Chiocchetti, A., Zhou, J., Zhu, H., Karl, T., Haubenreisser, O., Rinnerthaler, M., Heeren, G., Oender, K., Bauer, J., Hintner, H., et al. (2007). Ribosomal proteins Rpl10 and Rps6 are potent regulators of yeast replicative life span. Exp. Gerontol. *42*, 275–286.
48. Nguyen, Y.H., Mills, A.A., and Stanbridge, E.J. (1998). Assembly of the QM protein onto the 60S ribosomal subunit occurs in the cytoplasm. J. Cell. Biochem. *68*, 281–285.
49. Shen, B., Zhang, J., Wu, H., Wang, J., Ma, K., Li, Z., Zhang, X., Zhang, P., and Huang, X. (2013). Generation of gene-modified mice via Cas9/RNA-mediated gene targeting. Cell Res. *23*, 720–723.
50. Shen, B., Zhang, W., Zhang, J., Zhou, J., Wang, J., Chen, L., Wang, L., Hodgkins, A., Iyer, V., Huang, X., and Skarnes, W.C. (2014). Efficient genome modification by CRISPR-Cas9 nickase with minimal off-target effects. Nat. Methods *11*, 399–402.
51. Wang, H., Yang, H., Shivalila, C.S., Dawlaty, M.M., Cheng, A.W., Zhang, F., and Jaenisch, R. (2013). One-step generation of mice carrying mutations in multiple genes by CRISPR/Cas-mediated genome engineering. Cell *153*, 910–918.
52. Ittner, L.M., and Götz, J. (2007). Pronuclear injection for the production of transgenic mice. Nat. Protoc. *2*, 1206–1215.
53. Belin, S., Hacot, S., Daudignon, L., Therizols, G., Pourpe, S., Mertani, H.C., Rosa-Calatrava, M., and Diaz, J.J. (2010). Purification of ribosomes from human cell lines. Curr. Protoc. Cell Biol. *Chapter 3*. Unit 3.40.
54. Gandin, V., Sikström, K., Alain, T., Morita, M., McLaughlan, S., Larsson, O., and Topisirovic, I. (2014). Polysome fractionation and analysis of mammalian translatomes on a genome-wide scale. J. Vis. Exp. (87), e51455.
55. Peters, A.H., Plug, A.W., van Vugt, M.J., and de Boer, P. (1997). A drying-down technique for the spreading of mammalian meiocytes from the male and female germline. Chromosome Res. *5*, 66–68.

STAR★METHODS

KEY RESOURCES TABLE

REAGENT or RESOURCE	SOURCE	IDENTIFIER
Antibodies		
Rabbit polyclonal anti-RPL10	Novus	Cat# NBP1-84037; RRID: AB_11007661
Rabbit polyclonal anti-γH2AX	Novus	Cat# NB100-384; RRID: AB_10002815
Rabbit polyclonal anti-RPL4	Proteintech Group	Cat# 11302-1-AP; RRID: AB_2181909
Rabbit polyclonal anti-RPL11	Proteintech Group	Cat# 16277-1-AP; RRID: AB_2181292
Rabbit polyclonal anti-RPL19	Proteintech Group	Cat# 14701-1-AP; RRID: AB_2181587
Rabbit polyclonal anti-RPL31	Proteintech Group	Cat# 16497-1-AP; RRID: AB_2181772
Rabbit polyclonal anti-RPS3	Proteintech Group	Cat# 11990-1-AP; RRID: AB_2180758
Rabbit polyclonal anti-RPS15	Proteintech Group	Cat# 14957-1-AP; RRID: AB_2180163
Rabbit polyclonal anti-NEK2	Proteintech Group	Cat# 24171-1-AP
Rabbit polyclonal anti-HSPA2	Proteintech Group	Cat# 12797-1-AP; RRID: AB_2119687
Rabbit polyclonal anti-CCNA1	Proteintech Group	Cat# 13295-1-AP; RRID: AB_2071993
Rabbit polyclonal anti-CKS2	Proteintech Group	Cat# 15616-1-AP; RRID: AB_2260671
Rabbit polyclonal anti-mCherry	Abcam	Cat# ab167453; RRID: AB_2571870
Rabbit polyclonal anti-β-Actin	Abcam	Cat# ab8227; RRID: AB_2305186
Mouse monoclonal anti-SYCP3	Abcam	Cat# ab97672; RRID: AB_10678841
Mouse monoclonal anti-PLK1	Abcam	Cat# ab17056; RRID: AB_443612
Mouse monoclonal anti-γH2AX	Millipore	Cat# 05-636; RRID: AB_309864
Rabbit polyclonal anti-PLZF	Santa Cruz	Cat# sc-22839; RRID: AB_2304760
Lectin PNA Conjugate (Alexa Fluor 568)	Thermo Fisher	Cat# L-32458
Goat Anti-Mouse IgG1 (Alexa Fluor 488)	Thermo Fisher	Cat# A-21121; RRID: AB_141514
Donkey Anti-Rabbit IgG H&L (Alexa Fluor 555)	Thermo Fisher	Cat# A-31572; RRID: AB_162543
Donkey Anti-Rabbit IgG H&L (HRP)	Abcam	Cat# ab6802; RRID: AB_955445
Goat Anti-Mouse IgG H&L (HRP)	Abcam	Cat# ab6789 RRID: AB_955439
Rabbit polyclonal anti-RPL10L	This study; [35]	N/A
Bacterial and Virus Strains		
*Trans*5α Chemically Competent Cell	TransGen Biotech	Cat# CD201
Chemicals, Peptides, and Recombinant Proteins		
Puromycin	Sigma	Cat# P9620
Blasticidin S hydrochloride	Sigma	Cat# 15205
Doxycycline	Sigma	Cat# D9891
Protease inhibtor cocktails	Roch	Cat# 04693159001
RNasin Ribonuclease Inhibitors	Promega	Cat# N2511
Cycloheximide	Sigma	Cat# C7698
RNase OUT	Invitrogen	Cat# 10777-019
PMSF Protease Inhibitor	Thermo Fisher	Cat# 36978
RNase A	Thermo Fisher	Cat# EN0531
VECTASHIELD Antifade Mounting Medium	Vector	Cat# H-1000
Critical Commercial Assays		
ClonExpress MultiS One Step Cloning Kit	Vazyme	Cat# C113
PrimeScript RT reagent kit with gDNA Eraser	TaKaRa	Cat# RR047A
In Situ Cell Death Detection Kit	Roche	Cat# 11684817910
Experimental Models: Cell Lines		
HEK293T	ATCC	Cat# CRL-3216; RRID: CVCL_0063
A549	ATCC	Cat# CCL-185; RRID: CVCL_0023

(*Continued on next page*)

Continued

REAGENT or RESOURCE	SOURCE	IDENTIFIER
HeLa	ATCC	Cat# CCL-2; RRID: CVCL_0030
U-2 OS	ATCC	Cat# HTB-96; RRID: CVCL_0042
HCT116	ATCC	Cat# CCL-247; RRID: CVCL_0291
NIH/3T3	ATCC	Cat# CRL-1658; RRID: CVCL_0594
Mouse primary embryonic fibroblasts	This study	N/A
Experimental Models: Organisms/Strains		
C57BL/6 mouse	Beijing Vital River Laboratory Animal Technology Co.	Cat# 213
DBA/2 mouse	Beijing Vital River Laboratory Animal Technology Co.	Cat# 214
ICR mouse	Beijing Vital River Laboratory Animal Technology Co.	Cat# 201
Rpl10l knockout mouse	This study	N/A
Rpl10-mCherry transgenic mouse	This study	N/A
Oligonucleotides		
Oligos for plasmids construction, sgRNA, genotyping, RT-PCR and qPCR listed in Table S4	This study	N/A
Human *RPL10* siRNA 5′-GTCATCCGCATCAACA AGAT-3′	This study	N/A
Recombinant DNA		
pST1374-NLS-flag-linker-Cas9	Gift from Dr. Xingxu Huang [49]	Addgene, 44758
pUC57-sgRNA	Gift from Dr. Xingxu Huang [50]	Addgene, 51132
pGL3-U6-sgRNA-PGK-puromycin	Gift from Dr. Xingxu Huang [50]	Addgene, 51133
pTRIPZ vector (Tet on)	Gift from Dr. Xiaoyuan Song	N/A
Software and Algorithms		
CRISPR DESIGN	Zhang Lab at MIT	http://crispr.mit.edu/
Other		

CONTACT FOR REAGENT AND RESOURCE SHARING

Further information and requests for resources and reagents should be directed to and will be fulfilled by the Lead Contact, Dr. Qinghua Shi (qshi@ustc.edu.cn).

EXPERIMENTAL MODEL AND SUBJECT DETAILS

Mice

The care and breeding of mice and all animal experiments were conducted according to the guidelines and approved by the Institutional Animal Care Committee of the University of Science and Technology of China. The C57BL/6, DBA/2 and ICR mouse strains were purchased from Beijing Vital River Laboratory Animal Technology Co.

Rpl10l mutant mice were generated using CRISPR/Cas9 genome editing as previously described [51]. To generate *Rpl10l* mutants, we co-injected Cas9 mRNAs and two single guide RNAs targeting exon 1 that were prepared as previously described [50] into B6D2F1 (C57BL/6 × DBA/2) zygotes, followed by embryo transfer into pseudo pregnant ICR females. Genomic DNA was extracted from tail biopsies from founder mice using the TIANamp Genomic DNA Kit (TIANGEN DP304) and analyzed using the EasyTaq system (TransGen Biotech, AP111) and Sanger sequencing with primers *Rpl10l*-Check-FW and *Rpl10l*-Check-RV. We crossed female founders to C57BL/6 mice. Founder female #10 had deletions in both *Rpl10l* alleles (70 and 72 bp, respectively), and founder female #12 had a 59 bp deletion in one allele. For subsequent experiments, we used F2 generation animals that were homozygous for the 70 bp deletion (strain 1) and the 59 bp deletion (strain 2).

To generate *Rpl10-mCherry* transgenic mice, the pmRpl10l-mRPL10-mCherry vector was digested with ApaLI and purified using the MinElute PCR Purification Kit (QIAGEN, 28004). Linearized DNA was microinjected into B6D2F1 mouse zygotes following standard protocols [52]. Founders were genotyped by EsayTaq PCR system using two sets of primer pairs, which were *Rpl10-mCherry*^{TG}-FW1 and *Rpl10-mCherry*^{TG}-RV1, and *Rpl10-mCherry*^{TG}-FW2 and *Rpl10-mCherry*^{TG}-RV2. Transgenic founder males were intercrossed with *Rpl10l*$^{-/-}$ females (Strain 1), and their offspring (F2 generation) was used for experiments. Primers for genotyping listed in Table S4.

Cell culture

HEK293T (ATCC, CRL-3216), A549 (ATCC, CCL-185), HeLa (ATCC, CCL-2), U-2 OS (ATCC, HTB-96), HCT116 (ATCC, CCL-247), NIH/3T3 (ATCC, CRL-1658) and mouse primary embryonic fibroblasts (MEF) cells were cultured in high-glucose Dulbecco's Modified Eagle's Medium (DMEM) with 10% FBS (GIBCO, 15140122), 100 U/ml penicillin and 100 μg/ml streptomycin (GIBCO, 16000044) and maintained at 5% CO2, ambient O2.

293T cells with endogenous *RPL10* knockout and stable expression of Tet-On inducible RPL10-EGFP were generated by co-transfection of the following plasmids: pST1374-NLS-flag-linker-Cas9, the *RPL10*-targeting sgRNA expression plasmid based on the pGL3-U6-sgRNA-PGK-puromycin vector, and pTRIPZ-RPL10-EGFP. After selection in medium supplemented with 2 μg/ml puromycin, 2 μg/ml blasticidin, and 500 ng/ml doxycycline for 2 weeks, GFP-positive clones were isolated and cultured in medium containing 500 ng/ml doxycycline. Protein expression was validated by western blot analysis. Using the same method, we also generated 293T cells with endogenous *RPL10* knockout and stable expression of Tet-On inducible RPL10L-EGFP. Control cell lines expressing endogenous *RPL10* were produced by transfection of empty pGL3-U6-sgRNA-PGK-puromycin vector.

METHOD DETAILS

Plasmids

The RPL10-EGFP expression vector driven by the human *RPL10* promoter (phRPL10-RPL10-EGFP) was constructed as follows. The upstream 1.4 kb DNA fragment of the human *RPL10* open reading frame was amplified using primers phRPL10-FW and phRPL10-RV. The human *RPL10* coding sequence (CDS) was cloned from total RNAs extracted from 293T cells by RT-PCR with primers hRPL10-FW and hRPL10-RV. The backbone sequence was amplified from pEGFP-N1 with primers EGFP-BB-FW and EGFP-BB-RV. After purification by agarose gel electrophoresis and gel extraction, the three fragments were mixed and ligated using a ClonExpress MultiS One Step Cloning Kit (Vazyme, C113) according to the manufacturer's protocol. Vectors phRPL10-RPL10L-EGFP and phRPL10-EGFP were generated using the same approach. Because human *RPL10L* is intronless, the *RPL10L* CDS was cloned from genomic DNA extracted from 293T cells.

To obtain Tet-On inducible human RPL10 or RPL10L expression constructs, RPL10-EGFP and RPL10L-EGFP fragments were amplified from phRPL10-RPL10-EGFP and phRPL10-RPL10L-EGFP vector, respectively, and inserted into pTRIPZ vector (a kind gift from Dr. Xiaoyuan Song) using AgeI and MluI restriction sites.

The DNA construct used for *Rpl10-mCherry* transgenic mice was constructed using the ClonExpress MultiS One Step Cloning Kit (Vazyme, C113) as described above. The upstream 2 kb DNA fragment of mouse *Rpl10l* open reading frame was amplified using primers pmRpl10l-FW and pmRpl10l-RV. Mouse *Rpl10* CDS was cloned from total RNAs extracted from testis by RT-PCR with primers mRPL10-FW and mRPL10-RV. The backbone sequence was amplified from pmCherry-N1, which was modified from pEGFP-N1 with primers mCherry-BB-FW and mCherry-BB-RV. To remove the ApaLI site in mCherry, a synonymous mutation (GTA) was introduced to replace the codon (GTG) of amino acid 21 of mCherry.

The pST1374-NLS-flag-linker-Cas9 (Addgene, 44758) [49], pUC57-sgRNA (Addgene, 51132) [50] and pGL3-U6-sgRNA-PGK-puromycin (Addgene, 51133) [50] vectors were kind gifts from Prof. Xingxu Huang. To generate sgRNA expression plasmids, paired synthetic oligonucleotides were annealed and cloned into the BsaI site of pUC57-sgRNA or pGL3-U6-sgRNA-PGK-puromycin vector.

The Takara PrimeStar system (R044A) was used for PCR. All plasmids were validated by Sanger sequencing. Primers for plasmids construction and sgRNA listed in Table S4.

Transfection and RNAi

Cells were passaged 2-3 times after thawing and should be transfected at 70%–80% confluency. Transfection of plasmid or siRNAs was performed using lipofectamine 3000 (Invitrogen). The target sequence of the human RPL10 siRNA was 5′-GTCATCCGCATCA ACAAGAT-3′.

RNA extraction, RT-PCR and qPCR

Total RNAs were extracted using TRIzol reagents (Takara, 9109) and cDNAs were synthesized from total RNAs using the PrimeScript RT reagent kit (TaKaRa, RR047A) according to the manufacturer's protocol. EasyTaq DNA Polymerase (TransGen Biotech, AP111) was used for RT-PCR. The PCR reactions were performed using the following cycle conditions: 3 min at 94°C, followed by 25∼30 cycles of 30 s at 94°C, 30 s at 60°C, and 30 s at 72°C. FastStart Universal SYBR Green Master (Rox) (Roche, 04913850001) was used for quantitative real-time PCR in a StepOne Real Time PCR System (Applied Biosystems). The PCR reactions were performed using the following cycle conditions: 10 s at 95°C, followed by 40 cycles of 5 s at 95°C, and 30 s at 60°C. The gene encoding beta-Actin (*Actb*) was used as an internal control. Changes in gene expression were determined using the comparative CT method. Primers for RT-PCR and qPCR listed in Table S4.

Ribosome purification

Ribosome purification was performed as previously described [53]. In brief, 1×10^7 cultured human cells or 5×10^6 purified late prophase spermatocytes of mice were harvested and resuspended in 300 μL buffer A (250 mM sucrose, 250 mM KCl, 5 mM $MgCl_2$, and 50 mM Tris-HCl (pH 7.4)) containing 5mM PMSF and 50U RNase OUT, and lysed in 0.7% NP-40 for 15 min on ice. Nuclei and

mitochondria were removed by two successive centrifugations at 750 × g and 12000 × g, respectively. The concentration of KCl in the supernatants was adjusted to 500 mM, and samples were deposited above a 1 M sucrose cushion containing 500 mM KCl. Ribosome pellets were obtained after ultracentrifugation at 75,000 rpm for 2 hr at 4°C in a TL100.3 ultracentrifuge (Beckman) and resuspended in 1 × SDS sample buffer, boiled for 10 min, and analyzed by western blot.

Protein samples and western blot analysis

Cells were washed with ice-cold PBS and lysed in 1 × SDS sample buffer (100 mM Tris-HCl pH 7.4, 2% SDS, 15% glycerol, 0.1% bromophenol blue and 5 mM dithiothreitol [DTT]). Cell lysates were denatured for 10 min and analyzed by western blot.

Protein samples were separated by SDS-PAGE and transferred to 0.45 μm pore size immobilon-P membranes (Millipore, IPVH00010) using a Tanon vertical electrophoresis and blotting apparatus (Tanon). Membranes were blocked in TBST buffer (50 mM Tris, pH 7.4, 150 mM NaCl and 0.5% Tween-20) containing 5% nonfat milk for 1 hr and incubated with primary antibodies diluted in TBST buffer containing 5% nonfat milk at 4°C overnight. Following incubation with horseradish peroxidase (HRP)-conjugated secondary antibodies (Abcam) for 1 hr, western blots were developed with chemiluminescence (GE Healthcare, ImageQuant LAS 4000). Primary antibodies were: anti-RPL10 (Novus Biological, NBP1-84037), anti-RPL4 (Proteintech, 11302-1-AP), anti-RPL11 (Proteintech, 16277-1-AP), anti-RPL19 (Proteintech, 14701-1-AP), anti-RPL31 (Proteintech, 16497-1-AP), anti-RPS3 (Proteintech, 11990-1-AP), anti-RPS15 (Proteintech, 14957-1-AP), anti-NEK2 (Proteintech, 24171-1-AP), anti-HSPA2 (Proteintech, 12797-1-AP), anti-CCNA1 (Proteintech, 13295-1-AP), anti-CKS2 (Proteintech, 15616-1-AP), anti-PLK1 (Abcam, ab17056), anti-β-actin (Abcam, ab8227) and Anti-mouse RPL10L [35].

Polysome profiling analysis

Polysome profiling analysis was performed as described previously [54]. Briefly, cultured cells were treated with 100 μg/ml cycloheximide for 5 min at 37°C in 5% CO_2, then washed twice with 10 mL of ice-cold 1 × PBS containing 100 μg/ml cycloheximide. The cells were scraped off gently in 5 mL of ice-cold 1 × PBS containing 100 μg/ml cycloheximide and were collected by centrifugation at 200 × g for 5 min at 4°C. After resuspension in 425 μL of hypotonic buffer (5 mM Tris-HCl (pH 7.5), 2.5 mM $MgCl_2$, 1.5 mM KCl and 1 × Protease inhibitor cocktails), lysates were centrifuged at 16,000 × g for 7 min at 4°C. Supernatants were applied to a 10%–50% sucrose gradient (containing 10 μg/ml cycloheximide, 0.1 × Protease inhibitor cocktails and 10 units/ml RNasin) and centrifuged in a SW41 rotor at 40,000 rpm for 2 hr at 4°C. Analysis and fractionation of polysome profiles was performed using a Density Gradient Fractionation Systems (Teledyne ISCO).

Flow cytometry

Cells were collected and incubated in 70% ice-cold methanol for 30 min, treated with RNase A (ThermoFisher, EN0531) and stained with propidium iodide (ThermoFisher, P1304MP), followed by analysis using a FACS Calibur flow cytometer (BD).

Separation of mouse spermatogenic cells

Spermatogenic cell populations were isolated using the STA-PUT method based on sedimentation velocity at unit gravity as previously described [26, 27]. Spermatogonia were isolated from 8 dpp mice. Preleptotene cells, leptotene and zygotene spermatocytes, and puberal pachytene spermatocytes were isolated from 18 dpp mice. Adult pachytene spermatocytes and round spermatids were isolated from adult mice (50-70 dpp).

Fertility test

Three adult males of each genotype were used for fertility test. Each male was mated with three wild-type C57BL/6 females. All the females were monitored for pregnancy. Litter dates, number of pups and sex ratios were recorded for all the resulting litters.

Histology

Testis sections were prepared as described [23]. For histological analysis, testes were fixed in 4% paraformaldehyde or Bouin's fixative overnight at 4°C. Samples were dehydrated through a graded series of ethanol, embedded in paraffin, serially sectioned, and stained with hematoxylin and eosin or periodic acid-Schiff. Slides were examined by light microscopy.

Sperm counting

Male mice were sacrificed by cervical dislocation. Epididymides, along with the vas deferens, were dissected and cut into small pieces in a tube containing 1 mL Dulbecco's Modified Eagle Medium (DMEM). Sperm were allowed to release into the medium during incubation at 37°C in a 5% CO_2 humidified incubator for 30 min. Sperm counts were determined using a hemocytometer.

Meiotic delay assay

Meiotic preparations were made as previously described [23]. Briefly, single-cell suspensions were prepared from isolated seminiferous tubule fragments in 2.2% (w/v) trisodium citrate dihydrate (isotonic solution) and centrifuged for 10 min at 800 rpm, followed by treatment with 0.9% (w/v) trisodium citrate dihydrate (hypotonic solution) for 12 min at 37°C and fixation in Carnoy's solution (75% methanol, 25% acetic acid) at 4°C. After three washes in fixative, chromosome preparations were made by dropping the cell

suspension onto cold slides. Slides were dried and stained with Giemsa. To determine meiotic delay, first meiotic metaphases (MMI) were counted in slide areas in which 1000 mid-pachytene nuclei were counted.

Spermatocyte micro-spreading and immunostaining

Spermatocyte chromosome preparations and immunofluorescence were performed as described previously [22, 55], with the following modifications. Slides were either used for immunofluorescence staining immediately or stored at −80°C. For immunofluorescence, slides were blocked for 30 min with 1 × phosphate-buffered saline (PBS) containing 3% nonfat milk. Slides were then incubated with primary antibodies against synaptonemal complex protein 3 (SYCP3) (Abcam, ab97672), γH2AX (Novus Biologicals, NB100-384), PLZF (H-300) (Santa Cruz, sc-22839) overnight at room temperature in a humidified chamber. Slides were then washed four to five times in 1 × PBS containing 0.1% Triton X-100. Secondary antibodies (Alexa Fluor 488 Goat anti-Mouse IgG and Alexa Fluor 555 Donkey anti-Rabbit IgG, Invitrogen) were applied for 1 hr at 37°C in a humidified chamber. Both primary and secondary antibodies were diluted in 1 × PBS containing 3% nonfat milk. After secondary antibody incubation, four to five washes were performed in PBST (1 × PBS containing 0.1%Triton X-100) and the slides were mounted with VECTASHIELD mounting medium (H-1000, Vector Laboratories). Images were captured using a BX61 microscope (Olympus) connected to a CCD camera and analyzed using the Image-Pro Plus software (Media Cybernetic).

TUNEL assay

Testis sections were deparaffinized using standard methods (xylene, absolute, 95, 90, 80, and 70% ethanol and sterile water) and permeabilized with proteinase K (20 μg/ml) in 10 mM Tris-HCl (pH 7.5) for 15 min at room temperature. After two washes with 1 × PBS, sections were blocked with 3% BSA and 10% normal donkey serum in 10 mM Tris-HCl (pH 7.5) for 30 min. Thirty μl of TUNEL reagent mix (In Situ Cell Death Detection Kit, Fluorescein, Roche, 11684795910) were applied to each slide followed by incubation for 60 min at 37°C according to the manufacturer's protocol. Sections were then washed with PBST (0.1% Triton X-100 in 1 × PBS) four times and mounted in VECTASHIELD mounting medium (H-1000, Vector Laboratories) containing Hoechst 33342 (Invitrogen, H21492). Images were captured using a Nikon ECLIPSE 80i microscope (Nikon) connected to a CCD camera (Hamamatsu) and analyzed using the NIS-Element Microscope imaging software (Nikon).

Immunostaining of testis sections

Immunostaining of testis sections was performed as described previously [23], with the following modifications. Testes were fixed in 4% paraformaldehyde for 6 hr, dehydrated in 30% sucrose (w/v) for at least 8 hr and embedded in OCT (Sakura Finetek, CA). Seven μm-thick sections were fixed for 20 min in pre-cold 4% paraformaldehyde (w/v) at room temperature and then washed twice in PBST (0.1% Triton X-100 in 1 × PBS). Sections were blocked in antibody dilution buffer (ADB) (10% normal donkey serum, 3% bovine serum albumin (BSA), 0.05% Triton X-100 in phosphate-buffered saline [PBS]) for 30 min, followed by an overnight incubation at 4°C with primary antibodies against mCherry (Abcam, ab167453) and γH2AX (EMD Millipore, clone JBW301, 05-636), or Lectin PNA (Alexa Fluor 568 Conjugate, Invitrogen, L32458). Four washes with PBST were performed prior to secondary antibody incubation (Alexa Fluor 488 Goat anti-Mouse IgG and Alexa Fluor 555 Donkey anti-Rabbit IgG, Invitrogen) at 37°C for 1 hr. Finally, sections were mounted in VECTASHIELD mounting medium (H-1000, Vector Laboratories) containing Hoechst 33342 (Invitrogen, H21492). Images were captured using a Nikon ECLIPSE 80i microscope (Nikon) equipped with a CCD camera (Hamamatsu) and analyzed using NIS-Element Microscope imaging software (Nikon).

QUANTIFICATION AND STATISTICAL ANALYSES

Quantitative proteomic analysis

Late prophase spermatocytes isolated from adult *Rpl10l*$^{+/+}$ and *Rpl10l*$^{-/-}$ mice were used for proteomic analysis by PTM Biolab (Hangzhou, China). Briefly, proteins were extracted from the samples by sonication in lysis buffer (8 M urea, 2 mM EDTA, 10 mM DTT and 1% Protease Inhibitor Cocktail) followed by precipitation with cold 15% TCA for 4 hr at −20°C. Approximately 100 μg protein from each sample was digested with trypsin for the following experiments. After digestion, peptides were labeled using the 6-plex TMT kit according to the manufacturer's protocol (*Rpl10l*$^{+/+}$-126, *Rpl10l*$^{+/+}$-127, *Rpl10l*$^{+/+}$-128, *Rpl10l*$^{-/-}$-129, *Rpl10l*$^{-/-}$-130 and *Rpl10l*$^{-/-}$-131). The peptide mixtures were fractionated by high pH reverse-phase HPLC using an Agilent 300 Extend C18 column (5 μm particles, 4.6 mm ID, 250 mm length) and combined into 18 fractions. Peptide fractions were then analyzed using a Q ExactiveTM hybrid quadrupole-Orbitrap mass spectrometer (ThermoFisher Scientific). The resulting MS/MS data were processed using the Mascot search engine (v.2.3.0). Tandem mass spectra were searched against the swissprot *Mus musculus* database. Trypsin/P was specified as cleavage enzyme allowing up to 2 missing cleavages. Mass error was set to 10 ppm for precursor ions and 0.02 Da for fragment ions. Carbamidomethylation of Cys was specified as fixed modification and oxidation of Met was specified as variable modification. For protein quantification, TMT 6-plex was selected in Mascot. FDR was adjusted to < 1%, peptide ion score was set ≥ 20, p value was set < 0.05 and only proteins identified with at least two unique peptides were accepted. The downregulated and upregulated proteins in late prophase *Rpl10l*$^{-/-}$ versus *Rpl10l*$^{+/+}$ spermatocytes are listed in Table S2.

Statistical analysis

Results are presented as mean ± SEM. All statistical analyses were performed using Student's t test. p values less than 0.05 were considered to be statistically significant. The following indications were used throughout the manuscript: *$p < 0.05$, **$p < 0.01$, ***$p < 0.001$, NS, $p > 0.05$.

DATA AND SOFTWARE AVAILABILITY

The online CRISPR DESIGN tool provided by Zhang's lab at MIT (http://crispr.mit.edu/) was used to design sgRNA for gene editing. The genome sequences and information of targeted genes were searched from the Ensembl genome browser database (http://asia.ensembl.org/index.html). The information listed in Table S1 was searched from the NCBI Gene database (http://www.ncbi.nlm.nih.gov/gene).